



Article

Quantifying Multi-Scale Performance of Geometric Features for Efficient Extraction of Insulators from Point Clouds

Jie Tang¹, Junxiang Tan^{1,*} , Yongyong Du², Haojie Zhao¹ , Shaoda Li¹, Ronghao Yang¹ , Tao Zhang¹ and Qitao Li³

¹ College of Earth Sciences, Chengdu University of Technology, Chengdu 610059, China; tangjie1593@stu.cdut.edu.cn (J.T.); zhaohaojie@stu.cdut.edu.cn (H.Z.); lisd@cdut.edu.cn (S.L.); yangronghao@cdut.edu.cn (R.Y.); taozhang@stu.cdut.edu.cn (T.Z.)

² Chengdu Power Supply Company, Chengdu 610041, China; 20141113016t@cqu.edu.cn

³ Upper Changjiang River Bureau of Hydrological and Water Resources Survey, Hydrology Bureau of Changjiang Water Resources Commission, Chongqing 400020, China; liqitao@stu.cdut.edu

* Correspondence: tanjunxiang18@cdut.edu.cn; Tel.: +86-158-8247-0872

Abstract: Insulator extraction from images or 3D point clouds is an important part of automatic power inspection by unmanned airborne vehicles (UAVs), which is vital for improving the efficiency of inspection and the stability of power grids. However, for point cloud data, many challenges, such as the diversity of pylon shape and insulator type, complex topology, and similarity of structures, were not tackled with the study of power element extraction. To efficiently identify the small insulators from complex power transmission corridor (PTC) scenarios, this paper proposes a robust extraction method by fusing multi-scale neighborhood and multi-feature entropy weighting. The pylon head is segmented according to the aspect ratio of horizontal slices following the locating of the pylons based on the height difference and continuous vertical distribution firstly. Aiming to quantify the different contributions of features in decision-making and better segment insulators, a feature evaluation system combined with information entropy, eigen entropy-based optimal neighborhood selection, and designed multi-scale features is constructed to identify suspension insulators and tension insulators. In the optimization step, a region erosion and growing method is proposed to segment complete insulator strings by enlarging the perspectives to obtain more object representations. The extraction results of 82 pylons with 654 insulators demonstrate that the proposed method is suitable for different pylon shapes and sizes. The identification accuracy of the whole line achieves 98.23% and the average F1 score is 90.98%. The proposed method can provide technical support for automatic UAV inspection and pylon reconstruction.

Keywords: insulator extraction; point clouds; power inspection; quantification; information entropy



Citation: Tang, J.; Tan, J.; Du, Y.; Zhao, H.; Li, S.; Yang, R.; Zhang, T.; Li, Q. Quantifying Multi-Scale Performance of Geometric Features for Efficient Extraction of Insulators from Point Clouds. *Remote Sens.* **2023**, *15*, 3339. <https://doi.org/10.3390/rs15133339>

Academic Editors: Francisco Javier Mesas Carrascosa, José Emilio Meroño-Larriva and María Jesús Aguilera-Ureña

Received: 31 May 2023
Revised: 25 June 2023
Accepted: 26 June 2023
Published: 29 June 2023



Copyright: © 2023 by the authors. Licensee MDPI, Basel, Switzerland. This article is an open access article distributed under the terms and conditions of the Creative Commons Attribution (CC BY) license (<https://creativecommons.org/licenses/by/4.0/>).

1. Introduction

Insulators are core components attached to high-voltage pylons and play a decisive role in supporting overhead conductors. Insulator inspection is an essential work in regular patrol inspection because they are prone to damage caused by extreme environments and self-degeneration. Likewise, insulators tend to be self-exploding and lose insulation following a surge due to switching and lightning sometimes, leading to discharge, short circuits, and large-scale power failure [1,2]. However, frequent defect detection is a challenging task mainly caused by the long mileage and complex geographic environments.

In recent years, with the rapid development of small unmanned aerial vehicles (UAVs), or UAV systems, became more flexible and low-cost, and then some traditional and heavy manual inspections were gradually replaced by UAVs [3]. UAV systems typically integrate with technologies of multiple remote sensing sensors, such as thermal cameras, optical cameras, and light detection, and ranging (LiDAR) systems are widely used to help periodically monitor the vast network of power lines, which are more convenient and economical

compared with traditional measures, such as helicopter and manual patrol [2,4]. Generally, due to inaccessible mountainous areas, the tall and multi-layer characteristics of transmission pylons and the small size of insulator components, close-range photography, and detailed path planning for the safety of UAVs are accepted. The camera can capture images taken at close range, which can provide abundant details to improve the accuracy and reliability of defect detection [5–7]. The LiDAR systems can directly and efficiently obtain high-precision terrain information and coordinates of inspection objects to build high-precision 3D maps. Furthermore, LiDAR offers more convenience, stability, and fewer limitations of environmental texture in the acquisition of target point clouds compared to photogrammetric methods. To that end, taking advantage of the fact that the LiDAR system can provide the location of inspection objects, once the insulators are segmented, the key points of inspection can be extracted to guide safety route planning to capture clear insulator images [5,8]. The segmented insulator point clouds are also helpful for high-precision insulator modeling and fine reconstruction of the pylons. Therefore, it is particularly important to accurately extract and locate the insulators from 3D point clouds.

Currently, insulator extraction from point clouds still relies on manual work, requiring repetitive and heavy operations; hence an automatic extraction method is desired. However, the data volume of vast power transmission corridors (PTCs) and external environmental objects affect efficiency. More importantly, their geometric features produce significant interference for the extraction of particularly small insulators. Insulators have connectivity with power lines and pylons from a large-scale perspective, but they have similar performance in terms of structures of electricity elements and pylons in 3D point clouds from a small-scale perspective. Especially when the pylon size becomes larger, the wider spacing of the tower structure results in more steel structures being similar to insulators. Moreover, automatic extraction algorithms are susceptible to complex topology structures and system noise. Studies showed that the use of multi-scale features can eliminate or mitigate the impact of noise and high similarity between different objects on extraction accuracy and robustness [9–13]. However, there are few reports on how to use multi-scale geometric features and perform fusion and quantitative evaluation of these features to solve the problems in insulator extraction.

Efficient, high-precision, and robust insulator extraction was not effectively addressed, so this paper proposes an automatic insulator extraction method by quantifying the multi-scale performance of geometric features. A pylon extraction method was introduced to exclude most of the non-nylon elements and improve efficiency [14]. For cases in which the connectivity and similarity with other structures and system noise jointly impact the high-precision result, the multi-scale features are utilized to obtain significant representations. Further, for cumbersome feature threshold selection brought by multi-scale features and the decisive role of inappropriate scale, a specific entropy weighting method (EWM) is introduced to quantify the different contributions of features in decision-making, which solves the above problems and achieves robust results. Finally, according to the string characteristics, a region erosion and growing algorithm is used to refine candidate insulator point clouds and obtain complete insulators, which introduces the concepts of morphology opening operation. The main contributions are:

- Applying multi-scale features to provide significant representations of shape and structure information, mitigating the impact of noise and similarity on extraction accuracy.
- Introducing the EWM to quantify the multi-scale performance of geometric features, producing robust results.
- Developing an automatic data-driven method to extract insulators from pylons with various shapes and sizes, where tension and suspension insulators can be distinguished as well.

This paper is outlined as follows: Section 2 reviews the state-of-art method related to insulator extraction using point cloud data. Section 3 introduces experiment datasets and describes the proposed approach in detail. Section 4 provides a sensitivity analysis

and experimental results. Section 5 analyzes the possible conditions and performance of multi-scale neighborhoods. Section 6 concludes this work and provides plans.

2. Relate Works

2.1. Insulator Extraction

Multiple solutions that focus on image-based insulator extraction and point cloud-based insulator extraction appeared for many years with continuous studies and their importance was repeatedly emphasized in related reviews [4,5,8,15]. Extracting insulators from images such as optical aerial images and thermal images is a hot topic with enormous practical significance. Some studies developed algorithms based on image processing to achieve accurate insulator segmentation [16–18]. Recently, many learning technologies were applied to insulator defect inspection, and the first step is to accurately locate the position of the insulator from the complex background [1,2,19–22]. Among these studies, one common problem is that the missing insulators in images reduce the accuracy. Moreover, the 3D location of faulty insulators cannot be determined by images alone, and high-resolution insulator images are also much desired. Therefore, an automatic way that can guide the taking of close photographs from multiple directions and can also be applied to periodic inspections will significantly improve the accuracy and efficiency of fault detection [8].

Point cloud-based power element extraction mainly focuses on objects with notable characteristics on large scales, such as power lines and pylons [14,23–26]. With the popularization and upgrading of LiDAR technology, the details of objects that the point cloud can express became richer, and they are widely used to extract other small electric tower components. Arastounia and Lichti proposed an approach based on a priori knowledge of the main directions to extract insulator point clouds in substation scenarios [27], and a subsequently improved method classified six types of components in which the insulators were extracted by detecting non-planar point clouds [28]. In the PTC scenario, Qin et al. extracted suspension insulators based on cylinder segment recognition by vertical angle and image processing from cable inspection robot (CLR) LiDAR data [29]. Ortega et al. proposed a contextual feature in the k-nearest neighbor point cloud and used verticality clustering to extract suspension insulators, only the tension insulators were not taken into account [24]. Zhang et al. identified the points between the end of power lines and the pylon center as tension insulators, which rely on multiple-stage preprocessing and the accuracy of power line extraction [14]. Guan et al. argued that the linear connector–tension insulator is easy to obtain after the segmentation of pylons and power lines based on the template matching approach [8]. However, they also concluded that it involves manual operations and usually aims for specific conditions.

All these studies seldom considered the type of insulators and the shape, size, and function of pylons, which differ in how the conductors or jump wires attach to them and how they distribute in different types of pylons, such as suspension and anchor. What is more, they did not evaluate absolute statistical accuracy. The reasons for this perhaps are that there are no standard performance metrics and poor data quality results in sparse insulator points. In our study, various pylons that differ in size, shape, type, and voltage level are taken into account, and we develop an automatic data-driven algorithm to accurately extract insulators in possible conditions.

2.2. Multi-Scale Feature Fusion

Multi-scale features can provide additional structural information and perform robustly in the presence of noise [12]. Brodu and Lague proposed a multi-scale dimensionality analysis that improves spatial resolution by combining multi-scale features, which perform better than a single scale, especially for small objects [13]. An appropriate neighborhood scale for each point could provide a more accurate prescription. Demantke et al. proposed an optimal neighborhood selection by determining scales when ones of linearity (1D), planarity (2D), and sphericity (3D) have the maximum proportion [30]. Weinmann et al. proposed an eigen entropy-based scale selection strategy, which chooses scales with

minimum eigen entropy, arguing that the optimal neighborhood improves the distinctiveness of features [31]. In the following review, the classification of wire and pole/trunk performs better than constant scales and dimensionality-based scale selection [32]. Huang et al. combined multi-scale geometrical features to provide a better representation of point clouds and revealed a classification improvement [33]. Si et al. fused multi-scale features to enrich contextual information, which significantly improved the denoising precision in urban areas [9]. Other recent studies were keen to use multi-scale for classification in classifiers and networks and brought positive and beneficial impacts [34–36]. In our study, the multi-scale neighborhoods and multiple features address the scale selection and improve the robustness when applied to small components.

3. Materials and Methods

3.1. Datasets

Insulators generally can be divided into two types based on their connection modes in overhead PTCs: suspension insulators (SIs) and tension insulators (TIs). As illustrated in Figure 1, the SIs colored in red are installed vertically under cross arms and utilized to hang power lines. The TIs rendered in blue are installed to horizontally mount on the cross arms and are used to withstand the lateral tension of power lines. Their distribution and length vary depending on pylon shapes, function, and PTC voltage. To test the performance of the proposed method in different pylon shapes and sizes, a large number of pylons are accessed and applied. Their details are listed in Table 1. The pylon (d) in higher-voltage PTCs has a larger size and longer insulators. The tension pylons have tension insulators, but some of this type of towers have suspension insulators, while others do not. The suspension pylons (g–j) have only suspension insulators. The T-type pylons (a–g) have different floors and sometimes asymmetry, and O-type pylons (h, i) have different insulator distributions. Although the portal pylon (j) has a simple shape, there are some linear structures similar to the insulators.

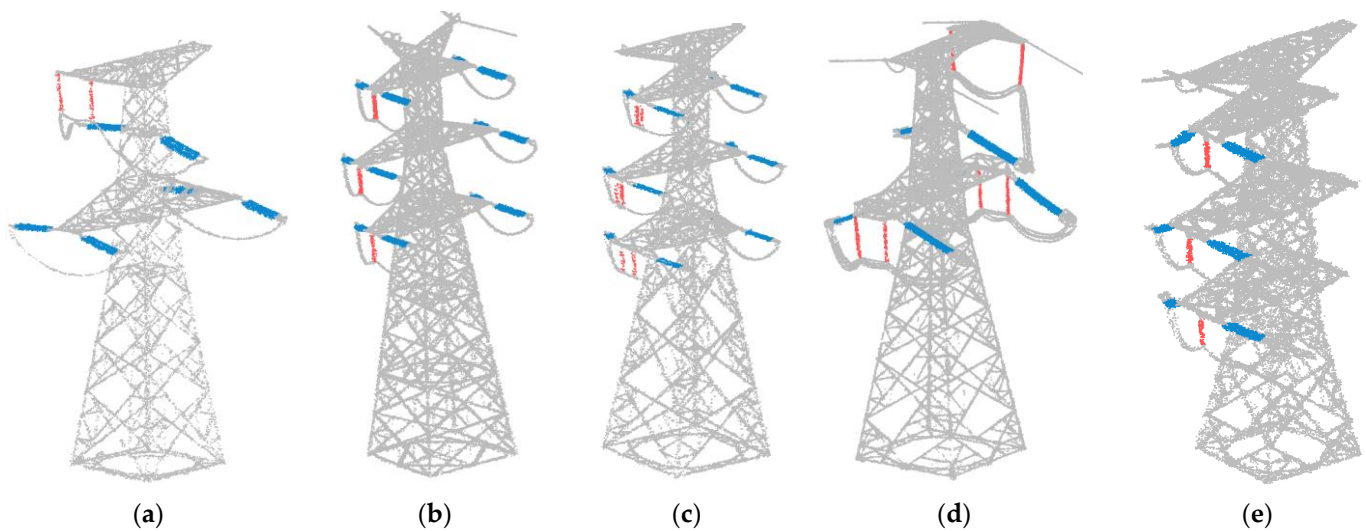


Figure 1. Cont.

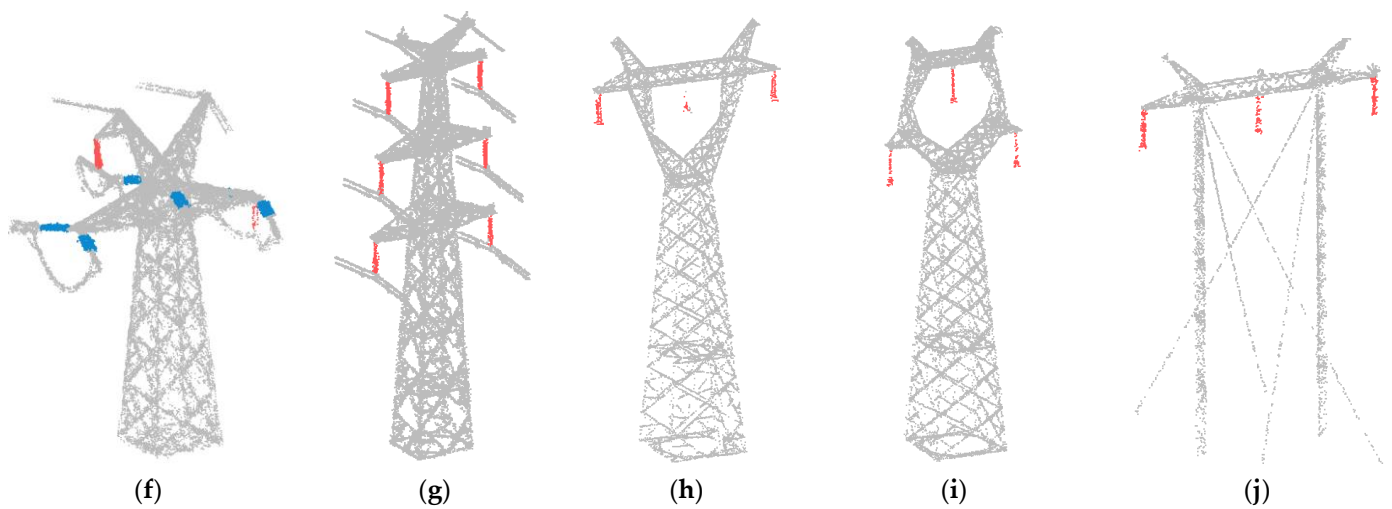


Figure 1. Pylon point clouds. (a–g) T-type pylons; (h,i) O-type pylons; and (j) a portal pylon. Suspension insulators are colored in red and tension insulators are colored in blue.

Table 1. Details of the power pylons.

Pylon	Length (m)	Width (m)	Height (m)	Number of SIs	Number of TIs
a	13.32	10.66	29.77	2	6
b	14.48	10.10	44.59	3	12
c	8.7	4.5	45.10	6	12
d	23.43	14.48	53.87	6	6
e	14.15	9.58	34.20	3	6
f	13.41	5.09	24.41	2	6
g	12.49	12.46	44.97	6	/
h	9.56	6.30	37.25	3	/
i	16.06	7.64	40.65	3	/
j	1.28	13.85	23.24	3	/

To test the accuracy of the proposed method in complete PTCs, we experimented with PTC point clouds acquired by using the CBI-300P (<http://www.a-lidar.com/Home> (accessed on 1 May 2023)) as shown in Figure 2. The CBI-300P with a laser scanner XT32 from HESAI (<https://www.hesaitech.com/cn/zh> (accessed on 1 May 2023)) is a centimeter-scale lightweight and high-precision LiDAR mapping system. There are 32 laser beams, higher point density, and less occlusion, which can provide more information on such small components as insulators. The relative accuracy is 5 cm and its scan rate is 1,920,000 points/s. The flight height is about 15 m above the power lines and the slant distance is about 15–30 m. It was widely used in power inspection thanks to its high precision and adaptability to multiple UAV platforms.

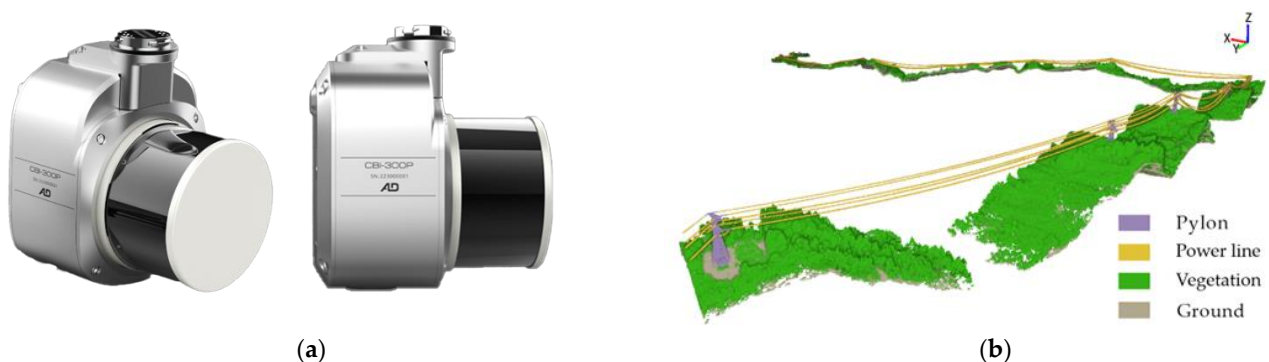


Figure 2. Device and dataset. (a) The CBI-300P LiDAR system and (b) point cloud data.

3.2. Methodology

A data-driven method is proposed to automatically extract insulators from PTC point cloud data. As shown in Figure 3, in the stage of extraction, pylons are detected from PTCs in the XOY plane and then the pylon heads with attachments installed are segmented to improve efficiency and reduce effects from the surrounding environment. After that, in the stage of multi-scale feature evaluation, according to the different types of insulators, two feature sets with multiple neighborhood scales are designed to extract both insulators and constrain the performance of other objects, and an entropy weighting system is added to obtain comprehensive scores. In the stage of refinement, the region erosion and growing algorithm is utilized to erode noises and grow the insulator along its principal direction. The results are complete point clouds of suspension insulator strings and tension insulator strings.

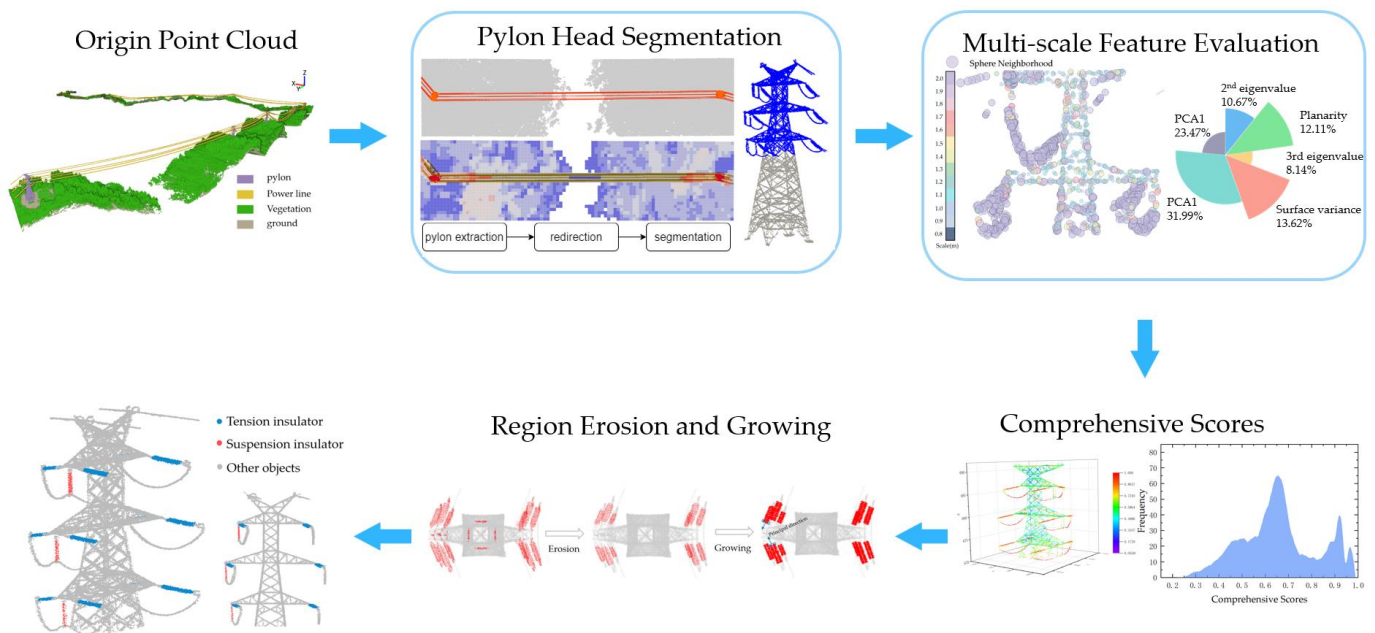


Figure 3. Workflow of the proposed method for insulator extraction.

3.2.1. Pylon Head Segmentation

It is difficult to extract such small insulators from vast PTCs with huge data volumes and to eliminate interference from surrounding environments. In the first step, an approach proposed by reference [14] is introduced to extract the pylons. The main ideas are illustrated in Figure 4, which identifies the pylons by analyzing features for whether there is continuous vertical distribution as shown in Figure 4a (the 2nd floor) and higher heights as shown in Figure 4a (the 3rd floor) in sparse grids, and then the centers are determined through vertical slice analysis. It can be seen that there is a larger relative height difference in the areas of power lines and pylons. Moreover, within these regions, the point clouds of pylons are dispersed across various height levels. The extraction results are pylon point clouds including the main bodies and components. Then, voxel sampling is utilized to further reduce the data volume of pylons and to make the point density more uniform without loss of details.

The pylon bodies with wider spacing structures could decrease the efficiency and potentially reduce the accuracy. Generally, most common pylon bodies have relatively regular quadrangular frustum pyramid structures. The XOY plane projection of their horizontal slices is a regular square. A characteristic of the square is that its aspect ratio is close to 1, which can be used to remove the horizontal slices until meeting the head with a lower aspect ratio as shown in Figure 4b. In special cases, the arbitrary orientation of pylons may result in head slices being incorrectly removed. A principal component analysis (PCA) algorithm is used to calculate the eigenvalues and eigenvectors of the point

clouds, in which an eigenvector corresponding to the maximum eigenvalue is the principal direction [37]. By rotating the X-axis to the principal direction around the Z-axis, the cross arms can be reoriented along the X-axis to prevent the insulators from being removed.

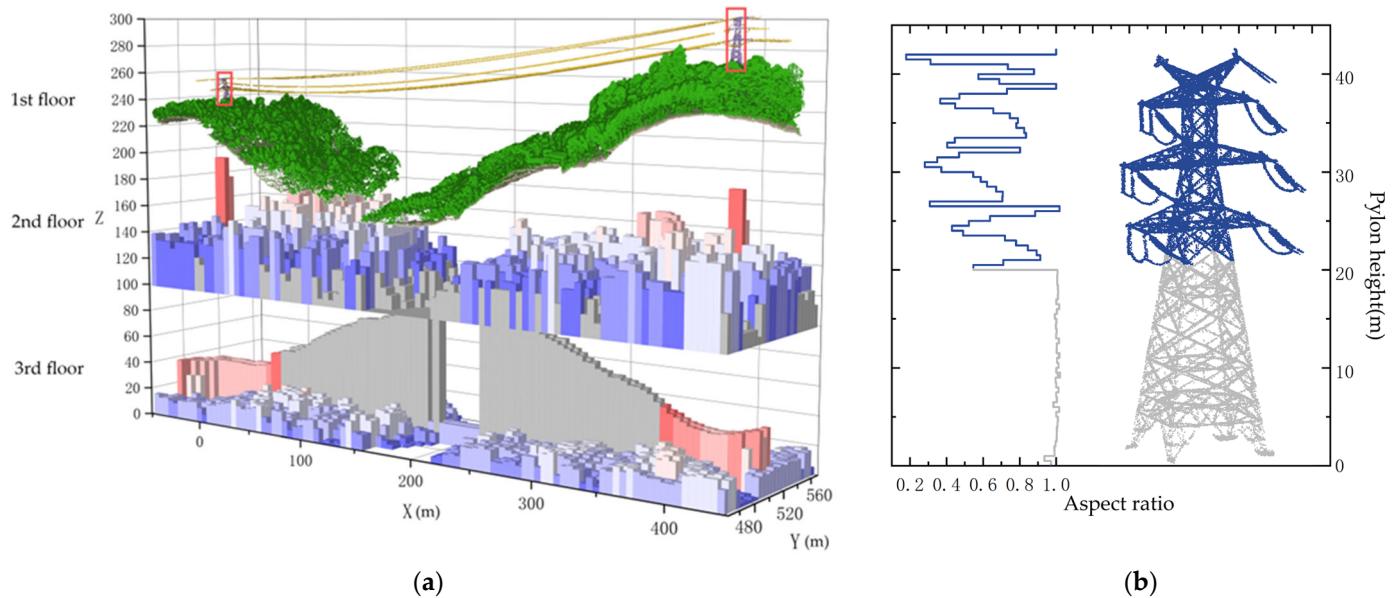


Figure 4. Process of pylon head segmentation. (a) Process of the pylon extraction. First floor: PTC point clouds, second floor: continuous vertical distribution, and third floor: height difference of point clouds in each sparse grid. (b) Head segmentation according to its aspect ratio.

3.2.2. Feature Construction

A specific feature cannot completely distinguish the insulators from other objects, but the constraint of multiple features can better classify the insulators. The structures of the pylon bodies and insulators are prone to having high linearity on a small scale, but the former has higher planarity on a larger scale. There is significant surface variation in the connection parts between both ends of the insulator and the pylons or power lines as well. On the strength of the above rules, by analyzing the object characteristics and connection mode, two different feature sets are designed to extract insulators including tension and suspension insulators. Limited by different scan distances and uneven point density, it is necessary to retrieve the radius sphere neighborhood to compute geometric features instead of k-nearest neighbors. The features are mainly divided into three categories: eigenvalue-based features, density features, and projection features. The designed features for different pylon types and details are listed in Table 2.

The eigenvalue features are widely used in feature estimation [32,38] and object extraction in the PTC scenario [23,24,39], which can better represent the local 3D shape features. For the tension insulators, the ME changes sharply as the neighborhood radius scale changes, which can be used for following multi-scale fusion. The SVs are significantly different from others at both ends of insulators, which can be used to remove the connection between insulators and other objects. The PCA1 and PCA2 are salient features for tension insulator extraction. The WI and PD are applied based on the specific characteristics of insulators for optimization. By rotating the principal direction of neighborhood point clouds to be in line with the X-axis, the width of the insulator string is usually between 0.6 m and 1.2 m. The suspension insulators have high VE compared with other objects. However, on small scales, other vertical structures complicate the extraction. The LS is used to distinguish suspension insulators that benefit from their simple surrounding distribution of point clouds. The PCA2 helps to accurately obtain linear structures such as suspension insulators.

Table 2. The designed features. The first column represents the feature categories, the second column represents the features, the third column listed the equations on how to compute these features, the fourth column represents applied features in TIs extraction, and the fifth column represents applied features in SIs extraction.

Category	Feature	Equation	TIs	SIs
Eigenvalue features	Minimum eigenvalue (ME)	λ_3	✓	
	Planarity (PL)	$(\lambda_2 - \lambda_3)/\lambda_1$	✓	
	Linearity (LI)	$(\lambda_1 - \lambda_2)/\lambda_1$	✓	
	Surface variation (SV)	$\lambda_3/(\lambda_1 + \lambda_2 + \lambda_3)$	✓	
	PCA1	$\lambda_1/(\lambda_1 + \lambda_2 + \lambda_3)$	✓	
	PCA2	$\lambda_2/(\lambda_1 + \lambda_2 + \lambda_3)$	✓	✓
	Verticality (VE)	$1 - \left (0, 0, 1) \bullet \vec{V}_1 \right $		
Density features	Point density (PD)	$num(\text{points})$	✓	
Projection features	Width (WI)	$Y_{\max} - Y_{\min}$	✓	
	Length–width Sum (LS)	$(X_{\max} - X_{\min}) + (Y_{\max} - Y_{\min})$		✓

Description: $\lambda_1, \lambda_2,$ and λ_3 ($\lambda_1 > \lambda_2 > \lambda_3$) represent the three eigenvalues calculated by the PCA algorithm. \vec{V}_1 represents the principal direction vector of the point cloud, and \bullet represents the dot operation. $X_{\max}, Y_{\max}, X_{\min},$ and Y_{\min} represent the maximum and minimum x and y coordinates, respectively.

3.2.3. Quantification of Multi-Scale Feature

The hierarchical thresholds of multiple features in extraction are commonly used, which set an empirical threshold for each feature step by step [11,24]. However, there are higher requirements for the performance of features and experience in the approach. As it is hard to find the optimal thresholds of features and error thresholds playing a decisive role, the EWM can better determine the contribution of each feature to the extraction that is desired to improve the robustness and flexibility. A concept called information entropy, which extended from the entropy theory proposed by Shannon, is applied to quantify the importance [40], which refers to the variation degree of indicators. If an indicator has a small information entropy, it means that the greater the variation degree it has, the more information it can provide, hence its weight is greater in decision-making. The EWM weakens the influence of abnormal values and makes the results more accurate and reasonable.

Insulators are particularly small, so it is difficult to find an appropriate neighborhood scale to exactly describe their characteristics, especially for such complex topology and similarity. The selection of radius parameters is fussy as well. Accordingly, applying small scales on small objects to accurately portray features while applying large scales to obtain more representation is desired for insulator extraction. The eigen entropy-based optimal neighborhood selection, which favored scales corresponding to the minimum eigen entropy, proved that the adoptive neighborhoods improved the distinctiveness of geometric features, especially for wire-like and pole/trunk-like objects [32]. The eigen entropy is calculated as Equation (1).

$$E = -\sum_{i=1}^3 e_i \ln e_i = -e_1 \ln(e_1) - e_2 \ln(e_2) - e_3 \ln(e_3) \quad (1)$$

where $e_1, e_2,$ and e_3 ($e_i = \lambda_i/\sum \lambda$) are normalized eigenvalues. The eigen entropy can represent the order/disorder of points within the local 3D neighborhood. The different performances of components at optimal neighborhood radius scales are shown in Figure 5, where the insulators tend to apply a larger neighborhood radius scale to accurately represent their linearity, while at the connection between insulators and other objects, the insulators tend to apply a small neighborhood radius scale to avoid being represented as other objects. The more complex pylon structures are applied with relatively small neighborhood scales.

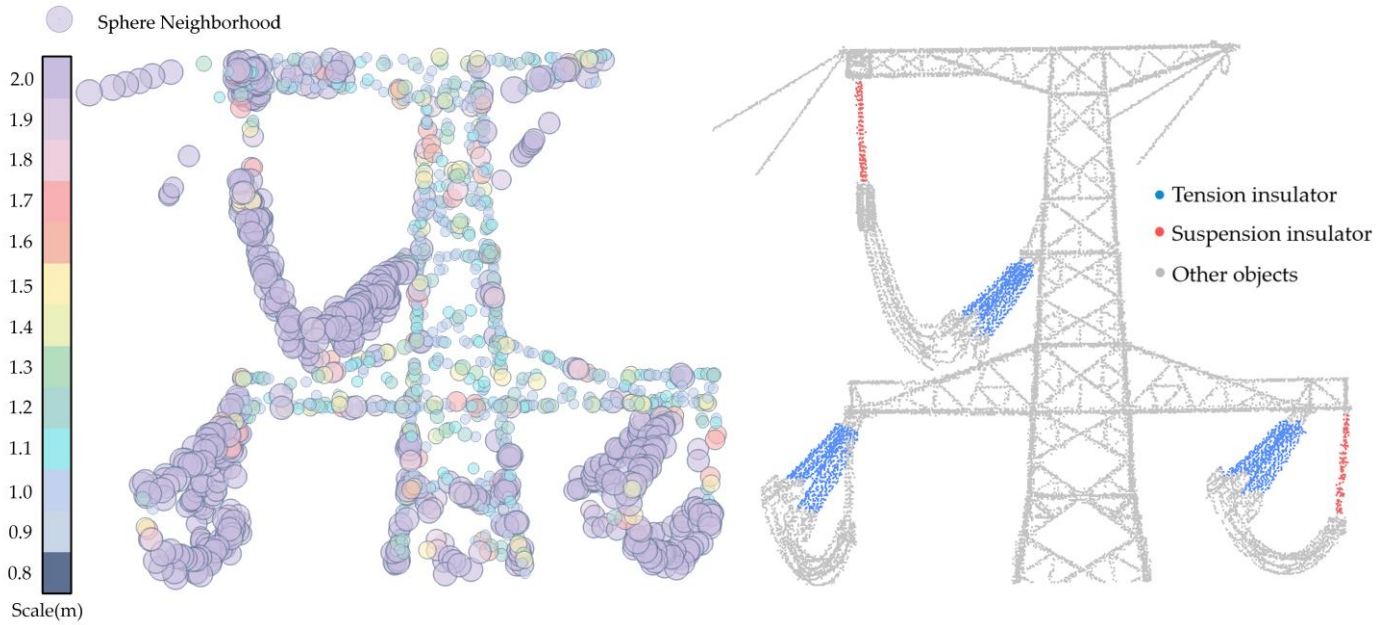


Figure 5. Performance of different components at optimal neighborhood radius scales.

An improved EWM is utilized, which combines with optimal neighborhood radius selection and multi-scale fusion. In the first step, the features (PCA2, SV, PCA1, and VE) corresponding to the optimal neighborhood radius should be extracted. We traversed the range of neighborhoods [0.8–2 m] with an interval of 0.1 m to compute the eigen entropy at each scale. Then, we selected the feature values of neighborhood radius scales corresponding to the minimum eigen entropy, noting that the steel bar structures of pylons and insulators perform high linearity on a small scale but the former perform high planarity on a larger scale. To obtain more representation, the ME within 0.8 m, LI within 1.3 m, and PL within 1.8 m are added to the feature matrix of tension insulators. The LS within 1.5 m is added to the feature matrix of suspension insulators. For cases in which there are different dimensions of features and their positive and negative contributions, the features should be normalized as Equation (2).

$$\begin{aligned} \text{negative feature} : \alpha_j &= \frac{v_{\max} - v_j}{v_{\max} - v_{\min}} \\ \text{positive feature} : \alpha_j &= \frac{v_j - v_{\min}}{v_{\max} - v_{\min}} \end{aligned} \tag{2}$$

where (v_{\min}, v_{\max}) , respectively, represent the minimum and maximum values of the feature and α_j represents the normalized value of the j -th point. For tension insulators, negative features, such as the ME, PL, PCA2, and SV, are distributed in a lower range. The positive features, such as PCA1 and LI, are distributed in a larger range. For suspension insulators, the negative features PCA2 and LS are distributed in a lower range, and the positive VE is distributed in a larger range. In this paper, we replace the normalization operation of negative features with “−” and replace the normalization operation of positive features with “+”. The feature evaluation for different types of insulators is shown in Equation (3).

$$S_{TI} = \begin{pmatrix} w_{ME} \\ w_{PL} \\ w_{PCA2} \\ w_{SV} \\ w_{PCA1} \\ w_{LI} \end{pmatrix}^T \cdot \begin{pmatrix} -\tilde{A}_{ME}(r \sim 0.8m) \\ -\tilde{A}_{PL}(r \sim 1.8m) \\ -\tilde{A}_{PCA2}(r \sim \min E_\lambda) \\ -\tilde{A}_{SV}(r \sim \min E_\lambda) \\ +\tilde{A}_{PCA1}(r \sim \min E_\lambda) \\ +\tilde{A}_{LI}(r \sim 1.3m) \end{pmatrix} \quad S_{SI} = \begin{pmatrix} w_{PCA2} \\ w_{LS} \\ w_{VE} \end{pmatrix}^T \cdot \begin{pmatrix} -\tilde{A}_{PCA2}(r \sim \min E_\lambda) \\ -\tilde{A}_{LS}(r \sim 1.5m) \\ +\tilde{A}_{VE}(r \sim \min E_\lambda) \end{pmatrix} \tag{3}$$

where w represents the weight of each feature, $\tilde{A} \sim (\alpha_1, \alpha_2, \dots, \alpha_n)$ represents the feature value sets, and $r \sim \min E$ represents the optimal neighborhood radius scale when minimum eigen entropy is reached. To obtain the weight of each feature, taking the feature evaluation of suspension insulators as an example, the information entropy of each feature should be calculated as Equation (1). Then, the final weights of features are calculated as Equation (4).

$$w_i = \frac{\frac{1}{\ln n - E(\tilde{A}_i)}}{\sum_{i=1}^6 \frac{1}{\ln n - E(\tilde{A}_i)}} \quad (4)$$

where $E(\tilde{A}_i)$ represents the information entropy of the i -th feature and n represents the number of values in the feature.

3.2.4. Optimize Extraction of Enlarged Perspective

In this stage, aiming to obtain complete insulator strings, most noise can be removed on the one hand, and then the perspective by growing point clouds can be enlarged to obtain more characteristics on the other hand. This operation can segment complete insulators while removing other objects through more characteristics. Noting that the candidate insulator point cloud extracted from the set interval contains noise points, while the noise points are different from the insulator points in some characteristics, the region erosion and growing method that introduces the concept of morphological opening operation [41] is proposed for optimization. Its basic ideas are: (1) Each type of insulator has fixed characteristics; for instance, width and high point density, which can be used to erode non-insulator points from the candidate insulator point cloud. (2) Growing along the principal direction of the insulator from both ends until meeting the junction of the pylon body or power line, the insulator point clouds can be completely extracted. Benefiting from the grown point clouds with more characteristics, such as verticality and length on a larger scale, the similarity with other objects will be further weakened. The steps are illustrated in Figure 6. We calculate the width and normalized point density of the spherical neighborhood point cloud of a 0.6 m radius for each point. Then, the points that do not belong to a set interval of width and point density can be removed and the remaining points are considered as points of the tension insulator. In our experiments, the width interval and the normalized point density range are set to 0.6–1.4 m and 0.6–1, respectively. After the erosion operation, we grow the cube region along the principal direction of each insulator from both of its ends until the cube point clouds belong to the pylon body or power line as shown in Figure 6c.

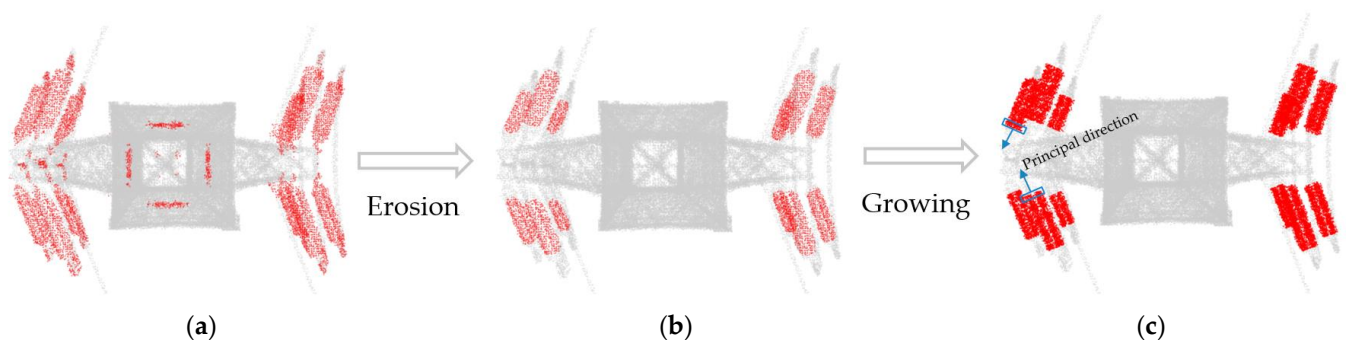


Figure 6. Region erosion and growing: (a) candidate insulator point clouds, (b) point clouds after erosion operation, and (c) point clouds after growing operation.

4. Results and Analysis

Recall, precision and F1-score are utilized to evaluate the extraction performance of our approach according to the past approach [9,23,39]. Likewise, we consider an insulator as correctly identified when the number of extracted insulator points is greater than half of the validation insulator. The identification rate is represented by Equation (5) [24].

$$R_i = \frac{n_{identified}}{n_{validation}} \quad (5)$$

where $n_{identified}$ represents the number of correctly identified insulators and $n_{validation}$ represents the number of validation insulators.

The proposed approach was mainly realized in Point Cloud Library Version 1.8.1 and Microsoft Visual Studio 2015. The program was operated on a computer with the Win 11 × 64 system, i5-12400H CPU, and NVIDIA GeForce RTX 3050Ti, and with general performance.

4.1. Parameters Analysis

In our approach, the input parameters are obtained in two different ways: most are adaptive and few are empirical. In the step of pylon head segmentation, we set the aspect ratio to 0.8 to completely remove the most common pylon bodies according to the experiments. The voxel sampling with a voxel of 0.2 m, which comes from experiments, is applied to obtain uniform point density while improving efficiency. In the step of EWM evaluation, the weight of each feature is determined by its contribution to decision-making. In a case where there are two different types of suspension insulators, twin and single, their characteristics are different from each other. Hence, we apply the normalized feature threshold scope instead of the fixed threshold scope to avoid misidentification. The neighborhood scales within a range of 0.8–2.0 would be discussed in 5.2. For the extraction threshold, they are obtained by traversing the comprehensive scores when there are the highest scores in 5.2. The comprehensive scores of tension insulators are mainly concentrated at 0.85–0.95 in the frequency distribution, and the comprehensive scores of suspension insulators are mainly concentrated at 0.8–1. In the step of optimization, we normalized the point density of insulator point clouds and set thresholds from 0.6 to 1 to erode non-insulator points.

4.2. Pylon Head Segmentation

Head segmentation can remove many useless parts while improving accuracy. Since our approach needs to find an optimal neighborhood for each point, the excessive points would seriously reduce efficiency, especially when applied to numerous pylons. Thus, it is an important part of improving efficiency and accuracy. For general pylons, their bodies are usually regular quadrangular frustum pyramids and the aspect ratio is close to 1 at any angle in each transversal slice. Even with the arbitrary orientation, the regular pylon body can be completely removed. However, the body of the portal pylon (j) is not a regular quadrangular frustum pyramid. Fortunately, thanks to the relatively simple structure, in the subsequent stage, its presence does not affect the final results of extraction. By testing the performance of pylon head segmentation on 82 pylons, 79 pylons are correctly segmented and 3 pylons are wrongly segmented. The wrong segmentation is due to the interference of power lines, where two insulators in one of the pylons are mistakenly removed by coincidence while the bodies in the other pylons are not removed. Pylons that are still over-segmented after they are reoriented indeed affect the final results, but in rare cases. By experimenting with the pylons where bodies fail to be removed, the insulators are still extracted correctly. The results of segmentation are illustrated in Figure 7. Except for the rare pylon shapes, the most common pylons perform better in head segmentation. On that basis, massive interferences are excluded and the rest come from pylon components only.

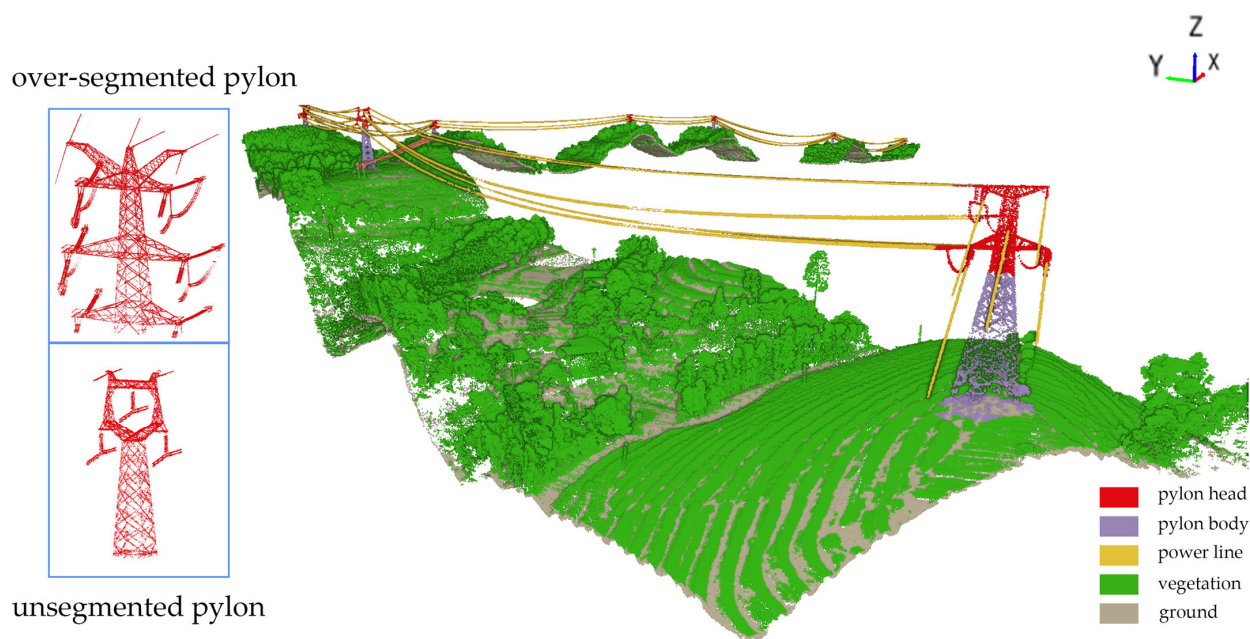


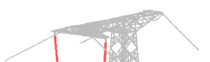
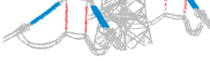
Figure 7. The results of pylon head segmentation.

4.3. Insulator Extraction

After the optimized extraction, the results and accuracy of tension insulators and suspension insulators for multiple pylon shapes are illustrated in Table 3. In general, the extraction accuracy of tension insulators is better, while the extraction accuracy of suspension insulators (pylon (c, f)) is sometimes reduced due to their fewer points. For such small components, fewer validation points would result in greater accuracy fluctuations than changes in correctly extracted points and falsely extracted points. For example, the point number of suspension insulators in pylon (c) and pylon (f) is 837 on average. However, in terms of length, 1.5 m-long insulators are extracted by 1.35 m in pylon (c), and 1.94 m-long insulators are extracted by 2.2 m in pylon (f). The end and center points regarded as key points for inspection would not deviate too far. Apparently, it can be seen that our approach is applicable to various pylon shapes and sizes. Regarding different voltage levels, such as 500 kv (pylon (d)) and 220 kv (pylon (a)), the former pylons and insulators are larger and longer than the latter. In terms of the benefits from the application of multi-scale neighborhoods and EWM, both have good results.

In our datasets, 82 pylons, which include 359 tension insulators and 295 suspension insulators, were tested. The processing efficiency is 0.08 million points per second. We consider an insulator as identified when half of its points are extracted. The recall and precision of identified tension insulators are 99.16% and 98.88%. The recall and precision of identified suspension insulators are 97.29% and 97.63%, respectively. The PTCs perform better thanks to the fact that the pylon shapes and sizes are not diverse. It is noteworthy that the poor results mainly include the following factors: (1) missing insulator points, and (2) very rarely, the similar performance of insulators and other objects in point clouds. As shown in Figure 8, when the insulator point clouds are not complete, they are not extracted because of the changed feature information. The missing insulator performs a higher linearity, resulting in a higher comprehensive score as shown in Figure 8a. With the current advantage of radar high density, such as with the CBI-300P system, this situation can be completely avoided. In another case, a few power lines are extracted when their characteristics, comprehensive scores, and point density are similar to the insulators. However, because the connected part is better removed, the power lines can be removed by setting a distance threshold from the pylon center as in reference [14]. In fact, for the existing research and algorithms with high accuracy on power line extraction, the results, such as in case (b), will be further improved after power lines are already extracted.

Table 3. Results and accuracy of the proposed approach for insulator extraction.

	Pylon	Accuracy of SIs	Accuracy of TIs	Pylon	Accuracy of SIs	Accuracy of TIs
Recall (%)		79.48	86.99		98.68	94.41
Precision (%)		98.39	96.56		60.01	97.30
F1-score (%)		87.93	91.52		74.63	95.83
Recall (%)		79.47	86.98		96.03	/
Precision (%)		98.39	94.61		96.53	/
F1-score (%)		87.93	90.63		96.27	/
Recall (%)		65.96	93.21		93.30	/
Precision (%)		100.00	98.52		97.92	/
F1-score (%)		79.49	95.79		95.55	/
Recall (%)		86.60	92.04		92.25	/
Precision (%)		99.31	99.82		100.00	/
F1-score (%)		92.52	95.78		95.97	/
Recall (%)		84.23	86.24		94.99	/
Precision (%)		100.00	99.23		89.30	/
F1-score (%)		91.45	92.28		92.05	/

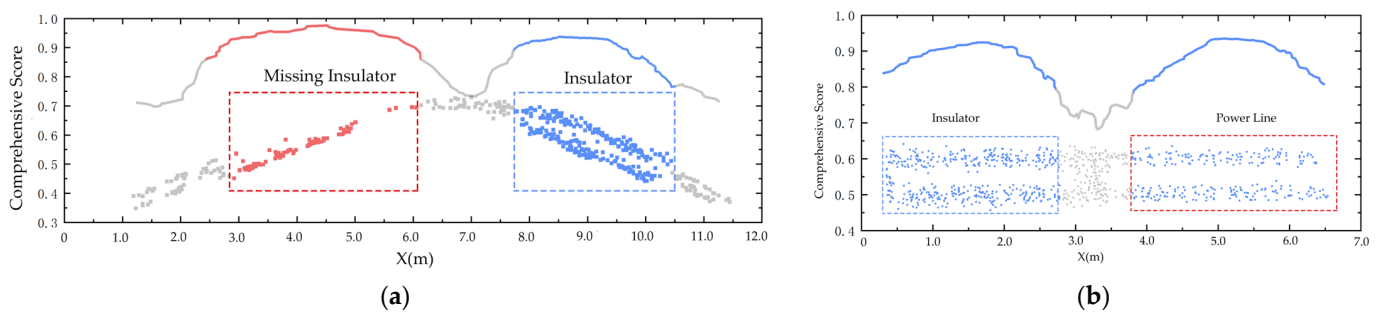


Figure 8. The cases of poor results. (a) The missing insulator case and (b) the high similarity case.

5. Discussion

5.1. Influences Come from Possible Conditions

Provided that there are three cases, poor point density, unusual pylon shape, and surrounding environment would potentially affect the extraction. Figure 9 presents some examples of extracted insulators and noise points. For poor point density, insulators usually contain only a few points and perform poor characteristics, which toughens their extraction. After testing several pylons with poor point density, as shown in Figure 9a, most insulator points are extracted. While twin power lines are also extracted due to the same performance as shown in Figure 9(a5). It can be avoided by pre-extracting power lines as illustrated in Figure 9(a4). For unusual pylons, comparing with the model-driven method, a data-driven approach with broad applicability to most possible insulator extractions is much desired. As shown in Figure 9b, the pylons are not common in PTCs; besides, the data quality is not very good. In these pylons, most insulators are correctly extracted. Partial pylon bodies are falsely extracted due to the similarity. It is noteworthy that three suspension insulators inside the pylon are extracted in such complex structures as Figure 9(b3), which means that the proposed approach is able to extract insulators with more complex distributions. There are too many insulators in the pylon as shown in Figure 9(b4). Every insulator is extracted, but the vertical structures complicate the extraction. Fortunately, their width is significantly greater than the width of insulators and can be removed in subsequent processing. For surrounding environments, because we extract pylon heads by roughly determining their centers on the XOY plane, the surrounding objects were not taken into account. Assuming that the failed pylon head segmentation would cause an accuracy decrease, Figure 9c shows some results and noise points. It can be seen that most interferences come from vertical trunks and poles. Some poles are extracted as seen in the green circle, and some insulators of terminal supports also are extracted as shown in the blue circle. A height and distance threshold is helpful to refine the results.

We conducted a point-wise estimation of the insulator extraction results and analyzed them under multiple pylon shapes and conditions in order to demonstrate a higher extraction accuracy and applicability than what is found in the existing literature. The reference [24] devised a pipeline for extracting suspension insulators. Some limitations of their method include the exclusion of tension insulators, reliance on power line extraction, and the experimental variation in the nearest neighbors parameter (n). They also argued that the point density could affect the final results. The references [8,14] briefly identify the transversal insulators between the end of power lines and pylons, which encounters difficulties when applied in scenarios involving unusual pylons, such as in Figure 9b and a complex environment such as in Figure 9c. Furthermore, they also impose higher requirements for pylon extraction and power line extraction.

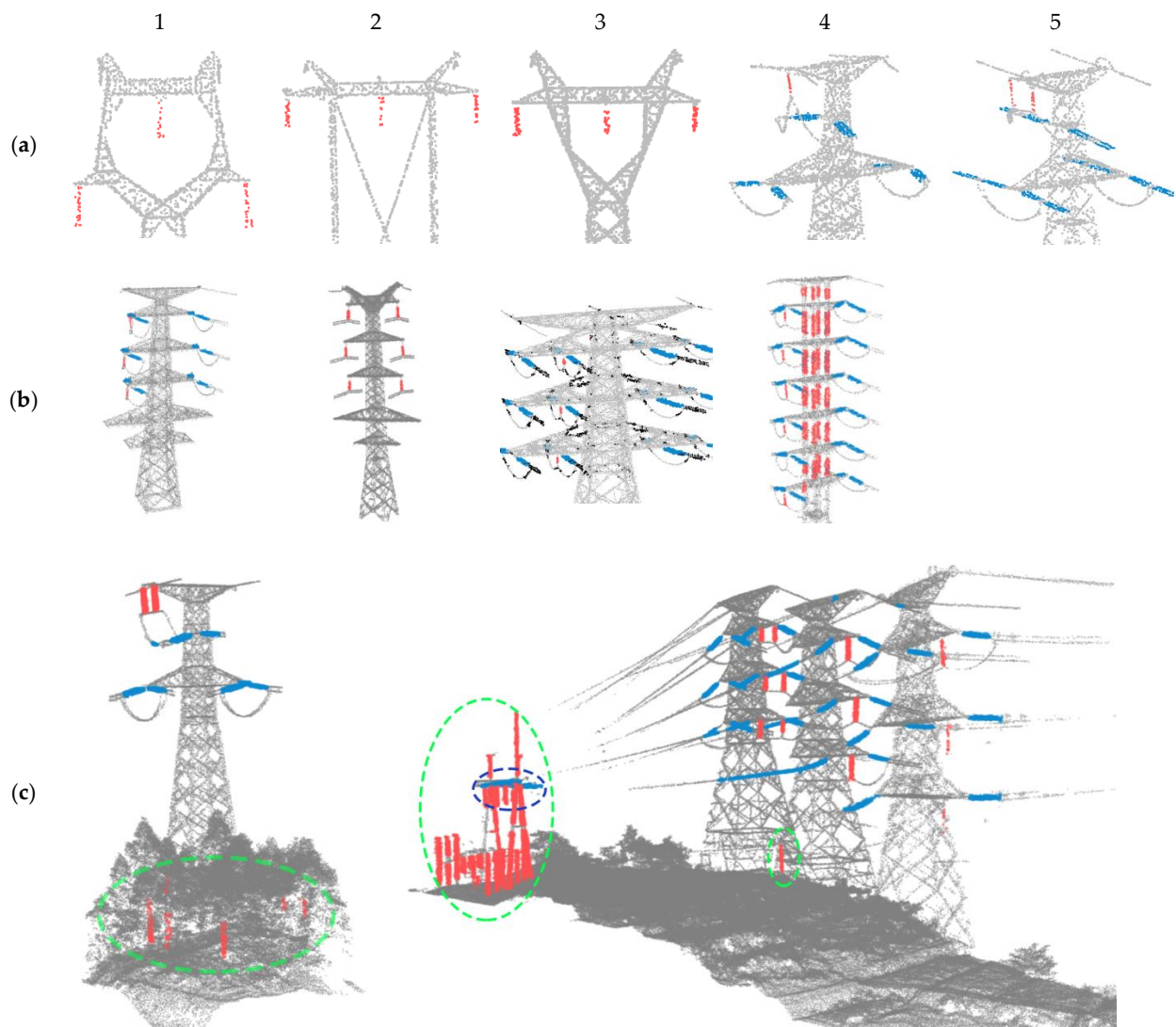


Figure 9. The proposed method applied to various conditions: (a) the sparse point density of pylons, (b) the unusual pylons, and (c) the complex environment. Suspension insulators are colored in red and tension insulators are colored in blue. Misidentified suspension insulators are marked in green circles and misidentified tension insulators are marked in blue circles.

5.2. Advantages of Multi-Scale Neighborhood

In this study, the shape and structure feature information of multiple scales is fused to extract insulators. To verify the improvements of multi-scale in the quantification, every single scale in a range [0.8–2.0 m] with an interval of 0.1 m, optimal neighborhood scale, and multi-scale fusion are tested on pylons from (a) to (f) with a tension insulator. Expecting more extraction and fewer omissions, a result with the highest F1-score is considered the best. The highest F1-score is obtained by traversing the comprehensive scores. They are illustrated in Figure 10.

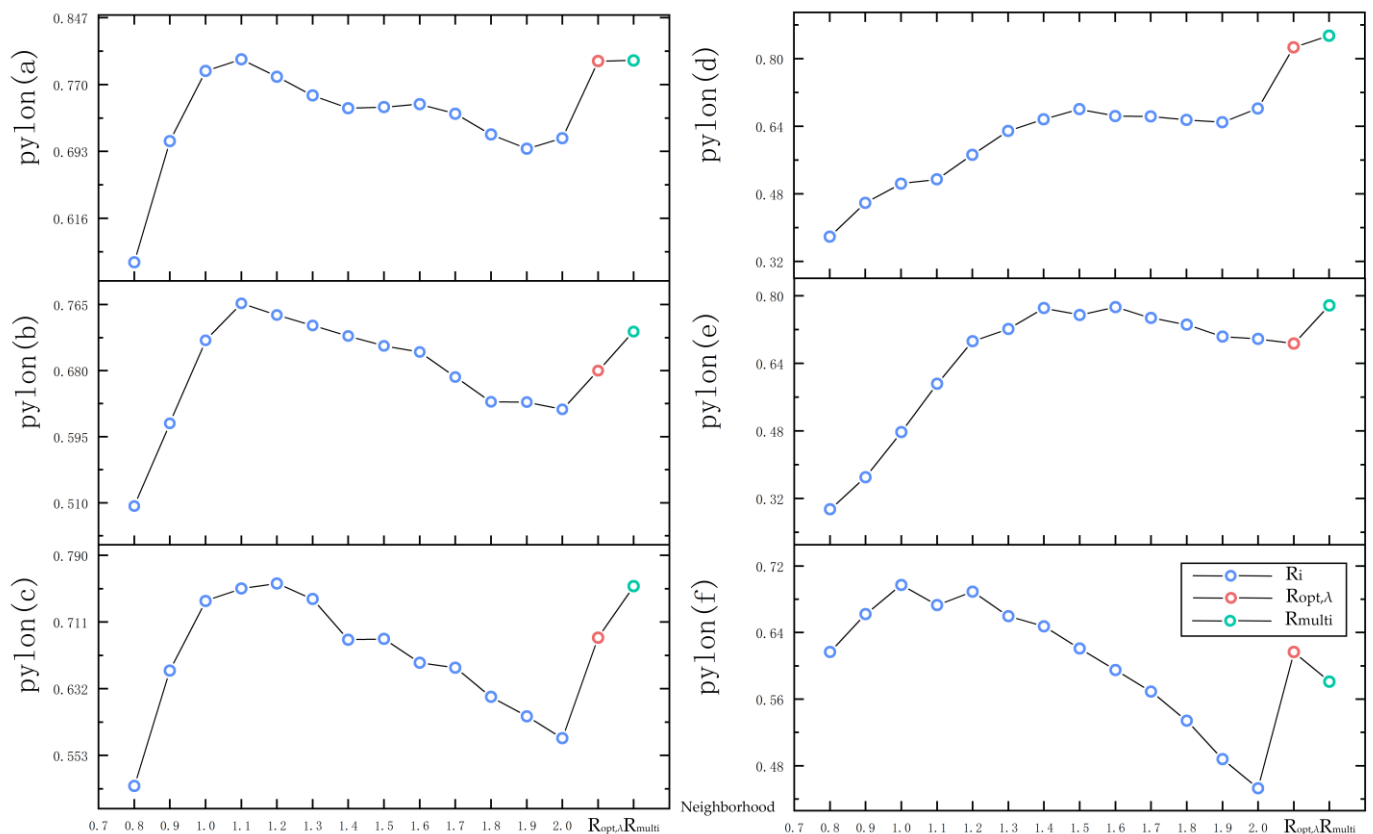


Figure 10. Performance evaluation of single-scale and multi-scale features. Description: $R_{opt,\lambda}$ represents the optimal neighborhood and R_{multi} represents the multi-scale neighborhood.

It can be seen that the extraction accuracy gradually increases and then decreases as the scale increases and perform sensitivity to scale changes. A scale of 1.1 m has the highest F1-score in pylon (a), but a scale of 1.5 m has the highest F1-score in pylon (d), indicating that a neighborhood scale with the highest accuracy changes in different pylons. It is clear that applying the same scale in different pylons will significantly reduce the accuracy, especially such small insulators. Through multi-scale feature fusion, the results consistently maintain a higher or the highest accuracy, avoiding the appropriate neighborhood scale selection and the decisive role of an inappropriate scale. What is more, taking advantage of the optimal neighborhood and multi-scale neighborhood, the results are significantly improved by 17.34% when extracting insulators in complex pylons such as pylon (d). A poor result in pylon (f) is mainly caused by excessive noise because we did not calculate features under optimal neighborhoods only. One reason for this is that the structures of pylons are prone to represent linearity and have smaller scales, so the features represented are relatively singular. The lower accuracy for optimal neighborhoods can prove that. These results highlight that the multi-scale neighborhood usually has wide applicability and higher accuracy.

6. Conclusions

In this paper, a data-driven insulator extraction method is proposed for various types of pylons and insulators. We discussed the complexity and the effect of scale change on insulator extraction. Pylon head segmentation, which locates the plane position of pylons and segment pylon heads by slices' characteristics, is a key step in reducing the data volume while improving accuracy. Then, the eigen entropy-based optimal neighborhood selection and multiple scales are fused to calculate various designed features and the information entropy-based weighting method improves the robustness of feature evaluation. The region erosion and growing method corrode the noise points and grow the principal direction,

which provides more representation of other objects, achieving a complete insulator string segmentation. The results given by the method tested on 82 different pylons are expected, with an F1-score of 99.12% for tension insulator extraction and an F1-score of 97.46% for suspension insulator extraction. The proposed method suggested that using the multi-scale neighborhood and different weights for features improved the applicability and robustness compared with the use of a constant neighborhood scale in related works.

This paper casts a new light on high-precision insulator extraction that should consider the effect of scales and point-based accuracy evaluation. However, there is a limitation in our study: it is difficult to completely constrain the representation of the linearity of the pylon structures, resulting in noise points in feature evaluation. Future lines of work will consider utilizing the cylinder neighborhood to calculate features instead of the current sphere neighborhood. According to the string characteristics of insulators, we expect that the cylinder neighborhood could bring more salient features. The balance of two parameters' radius and height complicates this intention. Another intention is to apply learning technologies to achieve higher accuracy.

Author Contributions: Conceptualization, J.T. (Junxiang Tan); investigation, J.T. (Jie Tang) and J.T. (Junxiang Tan); methodology, J.T. (Jie Tang), J.T. (Junxiang Tan), H.Z., S.L., R.Y. and T.Z.; resources, J.T. (Jie Tang), J.T. (Junxiang Tan), Y.D. and R.Y.; software, J.T. (Jie Tang), Y.D., H.Z. and T.Z.; supervision, J.T. (Junxiang Tan); validation, J.T. (Jie Tang) and J.T. (Junxiang Tan); visualization, S.L. and Q.L.; writing—original draft, J.T. (Jie Tang); writing—review and editing, J.T. (Jie Tang), J.T. (Junxiang Tan), Y.D., S.L., R.Y. and Q.L. All authors have read and agreed to the published version of the manuscript.

Funding: This research was funded by the Science and Technology Plan Project of Sichuan Province, grant number 2021YJ0369.

Data Availability Statement: Data is unavailable due to privacy or ethical restrictions.

Acknowledgments: We would like to thank Chengdu Alundar Technology, China, for providing the experimental data and to thank the anonymous reviewers for their valuable feedback.

Conflicts of Interest: The authors declare no conflict of interest.

References

1. Liu, J.; Liu, C.; Wu, Y.; Sun, Z.; Xu, H. Insulators' Identification and Missing Defect Detection in Aerial Images Based on Cascaded YOLO Models. *Comput. Intell. Neurosci.* **2022**, *2022*, 7113765. [[CrossRef](#)] [[PubMed](#)]
2. Ahmed, M.F.; Mohanta, J.C.; Sanyal, A. Inspection and identification of transmission line insulator breakdown based on deep learning using aerial images. *Electr. Power Syst. Res.* **2022**, *211*, 108199. [[CrossRef](#)]
3. Shakhathreh, H.; Sawalmeh, A.H.; Al-Fuqaha, A.; Dou, Z.; Almaita, E.; Khalil, I.; Othman, N.S.; Khreishah, A.; Guizani, M. Unmanned Aerial Vehicles (UAVs): A Survey on Civil Applications and Key Research Challenges. *IEEE Access* **2019**, *7*, 48572–48634. [[CrossRef](#)]
4. Yang, L.; Fan, J.; Liu, Y.; Li, E.; Peng, J.; Liang, Z. A Review on State-of-the-Art Power Line Inspection Techniques. *IEEE Trans. Instrum. Meas.* **2020**, *69*, 9350–9365. [[CrossRef](#)]
5. Matikainen, L.; Lehtomäki, M.; Ahokas, E.; Hyyppä, J.; Karjalainen, M.; Jaakkola, A.; Kukko, A.; Heinonen, T. Remote sensing methods for power line corridor surveys. *Isprs-J. Photogramm. Remote Sens.* **2016**, *119*, 10–31. [[CrossRef](#)]
6. Guo, L.; Liao, Y.; Yao, H.; Chen, J.; Wang, M. An Electrical Insulator Defects Detection Method Combined Human Receptive Field Model. *J. Control Sci. Eng.* **2018**, *2018*, 2371825. [[CrossRef](#)]
7. Nguyen, V.N.; Jenssen, R.; Roverso, D. Automatic autonomous vision-based power line inspection: A review of current status and the potential role of deep learning. *Int. J. Electr. Power Energy Syst.* **2018**, *99*, 107–120. [[CrossRef](#)]
8. Guan, H.; Sun, X.; Su, Y.; Hu, T.; Wang, H.; Wang, H.; Peng, C.; Guo, Q. UAV-lidar aids automatic intelligent powerline inspection. *Int. J. Electr. Power Energy Syst.* **2021**, *130*, 106987. [[CrossRef](#)]
9. Si, S.; Hu, H.; Ding, Y.; Yuan, X.; Jiang, Y.; Jin, Y.; Ge, X.; Zhang, Y.; Chen, J.; Guo, X. Multiscale Feature Fusion for the Multistage Denoising of Airborne Single Photon LiDAR. *Remote Sens.* **2023**, *15*, 269. [[CrossRef](#)]
10. Tang, Q.; Zhang, L.; Lan, G.; Shi, X.; Duanmu, X.; Chen, K. A Classification Method of Point Clouds of Transmission Line Corridor Based on Improved Random Forest and Multi-Scale Features. *Sensors* **2023**, *23*, 1320. [[CrossRef](#)]
11. Yang, B.; Dong, Z.; Zhao, G.; Dai, W. Hierarchical extraction of urban objects from mobile laser scanning data. *Isprs-J. Photogramm. Remote Sens.* **2015**, *99*, 45–57. [[CrossRef](#)]

12. Pauly, M.; Keiser, R.; Gross, M. Multi-scale Feature Extraction on Point-Sampled Surfaces. *Comput. Graph. Forum.* **2003**, *22*, 281–289. [[CrossRef](#)]
13. Brodu, N.; Lague, D. 3D terrestrial lidar data classification of complex natural scenes using a multi-scale dimensionality criterion: Applications in geomorphology. *Isprs-J. Photogramm. Remote Sens.* **2012**, *68*, 121–134. [[CrossRef](#)]
14. Zhang, R.; Yang, B.; Xiao, W.; Liang, F.; Liu, Y.; Wang, Z. Automatic Extraction of High-Voltage Power Transmission Objects from UAV Lidar Point Clouds. *Remote Sens.* **2019**, *11*, 2600. [[CrossRef](#)]
15. Miralles, F.; Pouliot, N.; Montambault, S. State-of-the-art review of computer vision for the management of power transmission lines. In Proceedings of the 3rd International Conference on Applied Robotics for the Power Industry, Foz do Iguacu, Brazil, 14–16 October 2014; pp. 1–6.
16. Wu, Q.; An, J.; Lin, B. A Texture Segmentation Algorithm Based on PCA and Global Minimization Active Contour Model for Aerial Insulator Images. *IEEE J. Sel. Top. Appl. Earth Observ. Remote Sens.* **2012**, *5*, 1509–1518. [[CrossRef](#)]
17. Liao, S.; An, J. A Robust Insulator Detection Algorithm Based on Local Features and Spatial Orders for Aerial Images. *Ieee Geosci. Remote Sens. Lett.* **2015**, *12*, 963–967. [[CrossRef](#)]
18. Li, W.; Ye, G.; Huang, F.; Wang, S.; Chang, W. Recognition of Insulator Based on Developed MPEG-7 Texture Feature. *Int. Congr. Image Signal Proc.* **2010**, *1*, 265–268.
19. Zhao, Z.; Zhen, Z.; Zhang, L.; Qi, Y.; Kong, Y.; Zhang, K. Insulator Detection Method in Inspection Image Based on Improved Faster R-CNN. *Energies* **2019**, *12*, 1204. [[CrossRef](#)]
20. Jiang, H.; Qiu, X.; Chen, J.; Liu, X.; Miao, X.; Zhuang, S. Insulator Fault Detection in Aerial Images Based on Ensemble Learning With Multi-Level Perception. *IEEE Access* **2019**, *7*, 61797–61810. [[CrossRef](#)]
21. Sampedro, C.; Rodriguez-Vazquez, J.; Rodriguez-Ramos, A.; Carrio, A.; Campoy, P. Deep Learning-Based System for Automatic Recognition and Diagnosis of Electrical Insulator Strings. *IEEE Access* **2019**, *7*, 101283–101308. [[CrossRef](#)]
22. Tao, X.; Zhang, D.; Wang, Z.; Liu, X.; Zhang, H.; Xu, D. Detection of Power Line Insulator Defects Using Aerial Images Analyzed With Convolutional Neural Networks. *IEEE Trans. Syst. Man Cybern. Systems* **2020**, *50*, 1486–1498. [[CrossRef](#)]
23. Jung, J.; Che, E.; Olsen, M.J.; Shafer, K.C. Automated and efficient powerline extraction from laser scanning data using a voxel-based subsampling with hierarchical approach. *Isprs-J. Photogramm. Remote Sens.* **2020**, *163*, 343–361. [[CrossRef](#)]
24. Ortega, S.; Trujillo, A.; Santana, J.M.; Suárez, J.P.; Santana, J. Characterization and modeling of power line corridor elements from LiDAR point clouds. *Isprs-J. Photogramm. Remote Sens.* **2019**, *152*, 24–33. [[CrossRef](#)]
25. Zhou, R.; Jiang, W.; Jiang, S. A Novel Method for High-Voltage Bundle Conductor Reconstruction from Airborne LiDAR Data. *Remote Sens.* **2018**, *10*, 2051. [[CrossRef](#)]
26. Awrangjeb, M. Extraction of Power Line Pylons and Wires Using Airborne LiDAR Data at Different Height Levels. *Remote Sens.* **2019**, *11*, 1798. [[CrossRef](#)]
27. Arastounia, M.; Lichti, D.D. Automatic extraction of insulators from 3D LiDAR data of an electrical substation. *ISPRS Ann. Photogramm. Remote Sens. Spat. Inf. Sci.* **2013**, *2*, 19–24. [[CrossRef](#)]
28. Arastounia, M.; Lichti, D. Automatic Object Extraction from Electrical Substation Point Clouds. *Remote Sens.* **2015**, *7*, 15605–15629. [[CrossRef](#)]
29. Qin, X.; Wu, G.; Lei, J.; Fan, F.; Ye, X. Detecting Inspection Objects of Power Line from Cable Inspection Robot LiDAR Data. *Sensors* **2018**, *18*, 1284. [[CrossRef](#)]
30. Demantké, J.; Mallet, C.; David, N.; Vallet, B. Dimensionality based scale selection in 3d lidar point clouds. *Int. Arch. Photogramm. Remote Sens. Spat. Inf. Sci.* **2012**, *38*, 97–102. [[CrossRef](#)]
31. Weinmann, M.; Jutzi, B.; Mallet, C. Semantic 3D scene interpretation: A framework combining optimal neighborhood size selection with relevant features. *ISPRS Ann. Photogramm. Remote Sens. Spat. Inf. Sci.* **2014**, *2*, 181–188. [[CrossRef](#)]
32. Weinmann, M.; Jutzi, B.; Hinz, S.; Mallet, C. Semantic point cloud interpretation based on optimal neighborhoods, relevant features and efficient classifiers. *Isprs-J. Photogramm. Remote Sens.* **2015**, *105*, 286–304. [[CrossRef](#)]
33. Huang, R.; Hong, D.; Xu, Y.; Yao, W.; Stilla, U. Multi-Scale Local Context Embedding for LiDAR Point Cloud Classification. *IEEE Geosci. Remote Sens. Lett.* **2020**, *17*, 721–725. [[CrossRef](#)]
34. Li, D.; Shi, G.; Wu, Y.; Yang, Y.; Zhao, M. Multi-Scale Neighborhood Feature Extraction and Aggregation for Point Cloud Segmentation. *IEEE Trans. Circuits Syst. Video Technol.* **2021**, *31*, 2175–2191. [[CrossRef](#)]
35. Wu, M.; Jiao, H.; Nan, J. Sparse 3D Point Cloud Parallel Multi-Scale Feature Extraction and Dense Reconstruction with Multi-Headed Attentional Upsampling. *Electronics* **2022**, *11*, 3157. [[CrossRef](#)]
36. Singh, S.; Sreevalsan-Nair, J. Adaptive Multiscale Feature Extraction in a Distributed System for Semantic Classification of Airborne LiDAR Point Clouds. *IEEE Geosci. Remote Sens. Lett.* **2022**, *19*, 1–5. [[CrossRef](#)]
37. Qiao, Y.; Xi, X.; Nie, S.; Wang, P.; Guo, H.; Wang, C. Power Pylon Reconstruction from Airborne LiDAR Data Based on Component Segmentation and Model Matching. *Remote Sens.* **2022**, *14*, 4905. [[CrossRef](#)]
38. Weinmann, M.; Jutzi, B.; Mallet, C. Feature relevance assessment for the semantic interpretation of 3D point cloud data. *ISPRS Ann. Photogramm. Remote Sens. Spat. Inf. Sci.* **2013**, *2*, 313–318. [[CrossRef](#)]
39. Tan, J.; Zhao, H.; Yang, R.; Liu, H.; Li, S.; Liu, J. An Entropy-Weighting Method for Efficient Power-Line Feature Evaluation and Extraction from LiDAR Point Clouds. *Remote Sens.* **2021**, *13*, 3446. [[CrossRef](#)]

40. Shannon, E.C. A Mathematical Theory of Communication. *Bell Syst. Tech. J.* **1948**, *27*, 623–656. [[CrossRef](#)]
41. Heijmans, H.J.A.M. Mathematical Morphology: A Modern Approach in Image Processing Based on Algebra and Geometry. *SIAM Rev.* **1995**, *37*, 1–36. [[CrossRef](#)]

Disclaimer/Publisher’s Note: The statements, opinions and data contained in all publications are solely those of the individual author(s) and contributor(s) and not of MDPI and/or the editor(s). MDPI and/or the editor(s) disclaim responsibility for any injury to people or property resulting from any ideas, methods, instructions or products referred to in the content.